Supporting Information

for

Hidden Oceans? Unraveling the Structure of Hydrous Defects in the Earth's Deep Interior

Helen Grüninger,[a] Katherine Armstrong,[b] Dominik Greim,[a] Tiziana Boffa-Ballaran,[b] Daniel J. Frost,*[b] and Jürgen Senker*[a]

[a] Anorganische Chemie III, Universitätsstrasse 30, University of Bayreuth, 95447 Bayreuth, Germany,

[b] Bayerisches Geoinstitut, Universitätsstrasse 30, University of Bayreuth, 95447 Bayreuth, Germany.

*To whom correspondence should be addressed;
Email: juergen.senker@uni-bayreuth.de; dan.frost@uni-bayreuth.de.

Contents

S1. Powder X-ray diffraction of ringwoodite and wadsleyite

Table S1: Lattice parameters after the multi-phase Rietveld refinement parameters of the PXRD of ringwoodite (Rwp = 4.49). The starting cell parameters and symmetry were taken from published crystallographic data of anhydrous ringwoodite, anhydrous stishovite and platinum.[1–3] An initial Pawley fit resulted in a Rwp value of 4.33, lattice parameter of a = 8.068 Å (ringwoodite) and a similar quality for the profile plot as observed for the Rietveld refinement (Figure 2).

Phase	*a / Å*	*b / Å*	*c / Å*	*α=β=γ / °*	*phase ratio*	*space group*	*Est. H_2O content / wt%*
Ringwoodite	8.0686(7)	8.0686(7)	8.0686(7)	90	97.94 %	$Fd\bar{3}m$	0.05-0.1
Stishovite	4.180(3)	4.180(3)	2.667(0)	90	1.42 %	$P4_2/mnm$	-
Platinum	3.884(0)	3.884(0)	3.884(0)	90	0.64 %	$Fm\bar{3}m$	

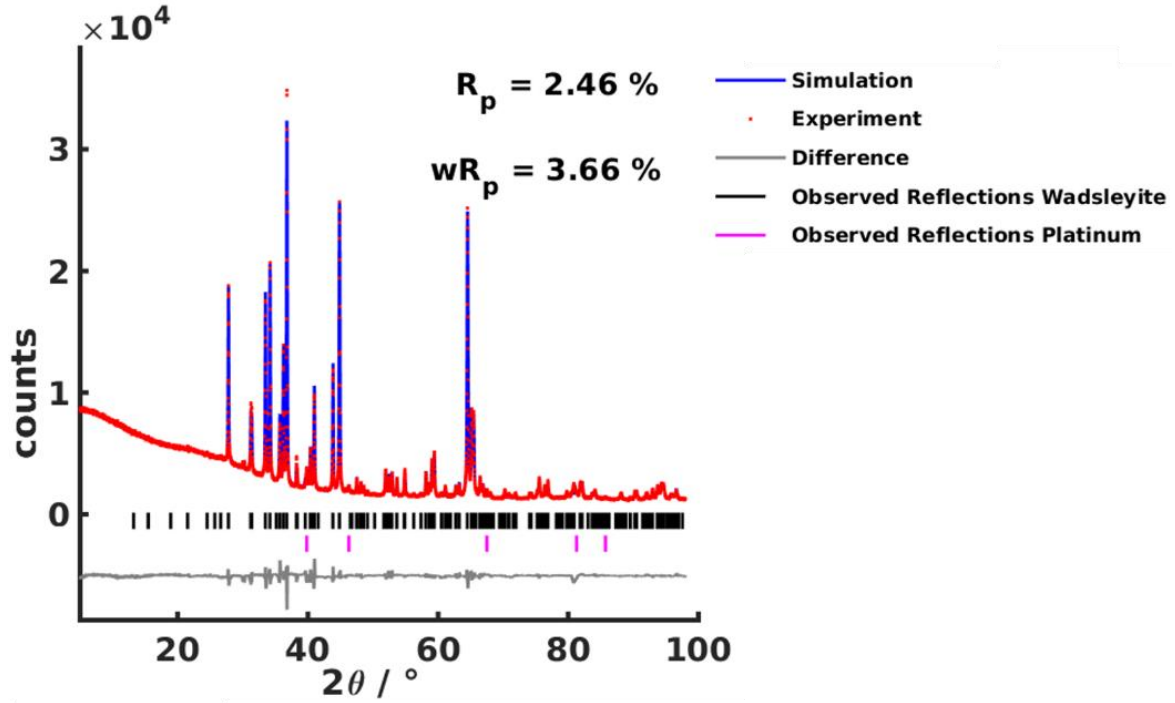

Figure S1: PXRD measurement of the hydrous wadsleyite sample (red) and the Rietveld refinement of wadsleyite and platinum (blue), respectively. The positions of the reflections of the individual phases, wadsleyite (black bars) and platinum (pink bars) are shown below the PXRD pattern. The refinement with a weighted profile R-value of 3.66 % gave a ratio of ~99.4% to ~0.6% between wadsleyite and a minor platinum impurity left from the capsule used in the synthesis. The determined lattice parameters for wadsleyite (space group Imma) are a=5.700(1) Å; b=11.449(2) Å; c=8.254(0) Å with α=β=γ=90° and for platinum (space group symmetry $Fm\bar{3}m$) a=b=c=3.921(8) Å with α=β=γ=90°. An initial Pawley fit resulted in a Rwp value of 2.92 and lattice parameters of a= 5.700(1) Å, b= 11.449(3) Å, c= 8.254(0) Å.

S2. ^{1}H ^{29}Si CPMAS ssNMR

The recorded ^{1}H-^{29}Si CPMAS spectra of ringwoodite with varying contact times of (2.5, 5.0, 10, 15 ms) are shown in Figure S2.

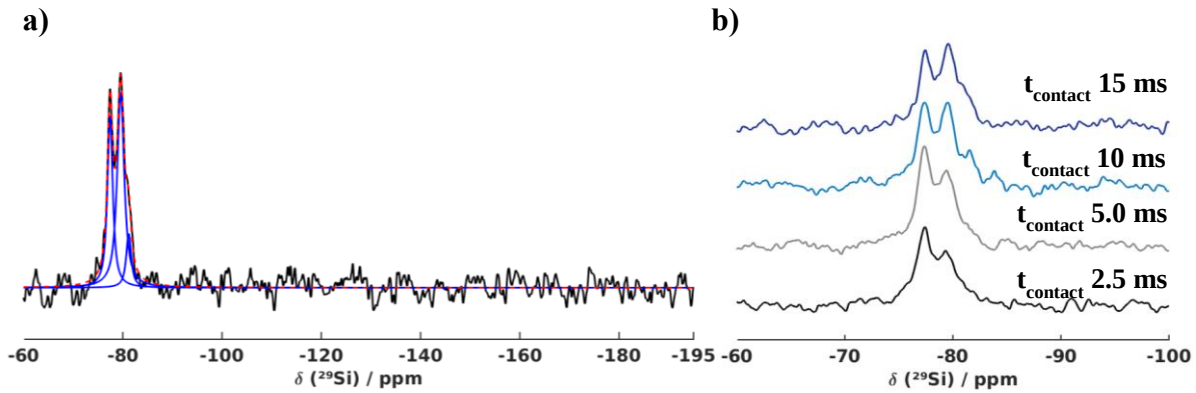

Figure S2: a) ^{1}H-^{29}Si CPMAS spectrum of ringwoodite resulting from coadding 32768 transients seperated by a recycle interval of 2.0 s. The contact pulse duration was set to 15 ms to make sure that also Si-species further away from protons would be excited. b) Comparison of the ^{1}H ^{29}Si CP MAS spectra of ringwoodite with different contact times.

S3. ^{1}H ssNMR

The parameters used for the fit of the 1D ^{1}H MAS spin echo (Figure 5a) are given in Table S2.

Table S2: Parameters of the fit of the 1D ^{1}H MAS spin echo shown in Figure 5a.

Signal	*δ_{iso} / ppm*	*FWHM / ppm*	*Relative integrals*	*Percentage / %*	*Assignment*
1	9.7	0.8	0.33	8.7 %	Si-OH
2	9.1	0.8	0.24	6.3 %	Si-OH
3	8.6	1.1	0.34	8.9 %	Si-OH
4	7.75	1.1	0.26	6.7 %	Si-OH
5	7.1	1.1	0.22	5.8 %	Si-OH
6	6.0	1.1	0.15	3.4 %	Si-OH / Mg-OH
7	4.9	1.1	0.30	7.9 %	Mg-OH
8	4.2	1.1	0.21	5.6 %	Mg-OH
9	3.5	1.1	0.16	4.2 %	Mg-OH
10	2.8	1.1	0.12	3.1 %	Mg-OH
11	2.2	1.1	0.17	4.4 %	Mg-OH
12	1.2	0.3	0.24	6.2 %	surface OH-species
13	1.2	1.1	1.00	25.9 %	Mg-OH
14	0.8	0.3	0.09	2.4 %	surface OH-species

The MAS spin echo spectra recorded with a MAS rate of 40 kHz and 62.5 kHz are almost identical (Figure S3), demonstrating that not the homonuclear dipolar coupling but the chemical shift distribution is the dominating factor.

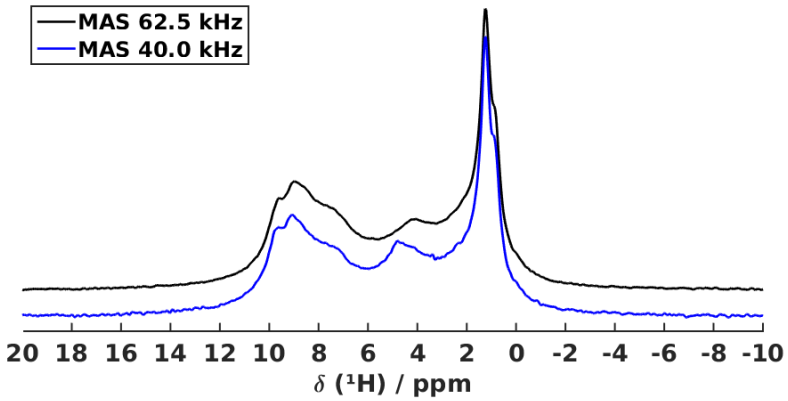

Figure S3: Comparison of ^{1}H MAS spin echos recorded at a MAS rate of 62.5 kHz (black) and 40.0 kHz (blue), respectively. The spectra are each the result of coadding 64 transients seperated by a recycle interval of 3.0 s.

Four rotor-synchronised 2D ^{1}H ^{1}H DQSQ MAS NMR spectra of our ringwoodite sample are shown in Figure S4. The spread along the diagonal ($\delta_{DQ} = 2\ \delta_{SQ}$) indicates a distribution of different hydroxyl proton environments. In addition to the autocorrelation signals along the diagonal, cross correlation signals at δ_{DQ}=6.5 ppm, δ_{DQ}=9.4 ppm and δ_{DQ}= 11.5 ppm were observed (Figure S4, dashed lines).

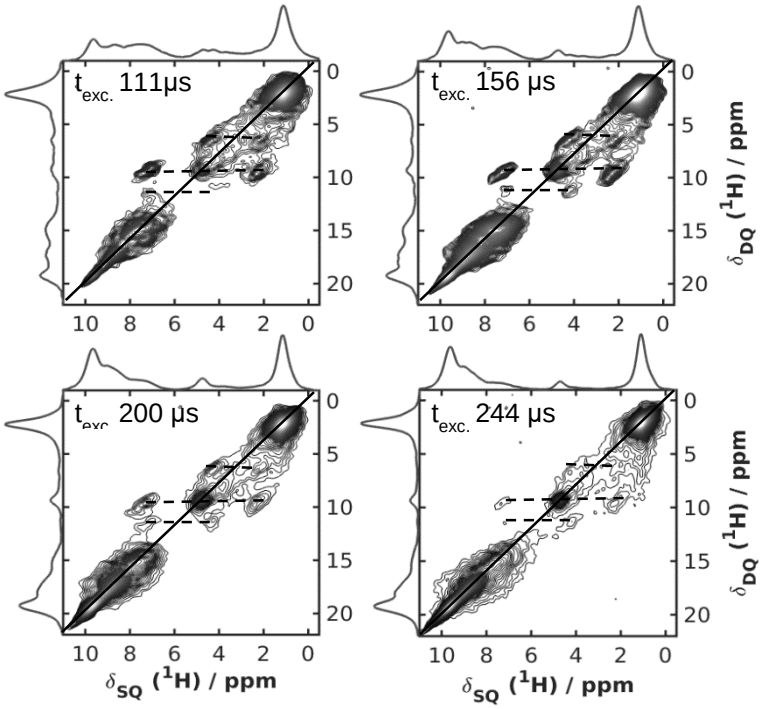

Figure S4: Rotor-synchronised ^{1}H ^{1}H DQSQ MAS NMR spectra were recorded using the $R18_8^5$ sequence with a S_0S_π supercycle.[4,5] The RR' Blocks were incremented to yield the excitation times $t_{exc.}$ of 111.11 µs, 155.56 µs, 200.00 µs (corresponding to one full $R18_8^5$ cycle) and 244.44 µs. DQ cross correlations are indicated by dashed lines. The ^{1}H ^{1}H DQSQ MAS NMR spectra are the results of sampling 256 transients seperated by a recycle interval of 2.0 s for each of the 132 t_1 increments of 50.00 µs. The spectra were recorded at a MAS rate of 40.0 kHz.

S4. Hydrous defect structures in ringwoodite used for DFT calculations

In the following a structural description of the six different hydrous defect types shown in Figure 3 with multiple proton configurations is given.

Isolated defects of the type V_{Mg}''+ 2H**, V_{Si}''''+ 4H**** and Mg_{Si}''+ 2H** are shown in Figures 3a-c and S5. For the case of the V_{Mg}''+ 2H** defect (Mg1) one Mg atom was removed from the octahedral 16d site and two protons were placed in the resulting vacant octahedron on opposite O atoms which was shown to be energetically favoured.[6] The resulting hydroxyl groups are in a mixed cation environment of two Mg and one Si cation and form hydrogen bridges (2.04 Å) along the shorter O-O edge shared by the 16d with its neighbor 16c octahedron which is vacant in the normal spinel structure (Figure S5a).

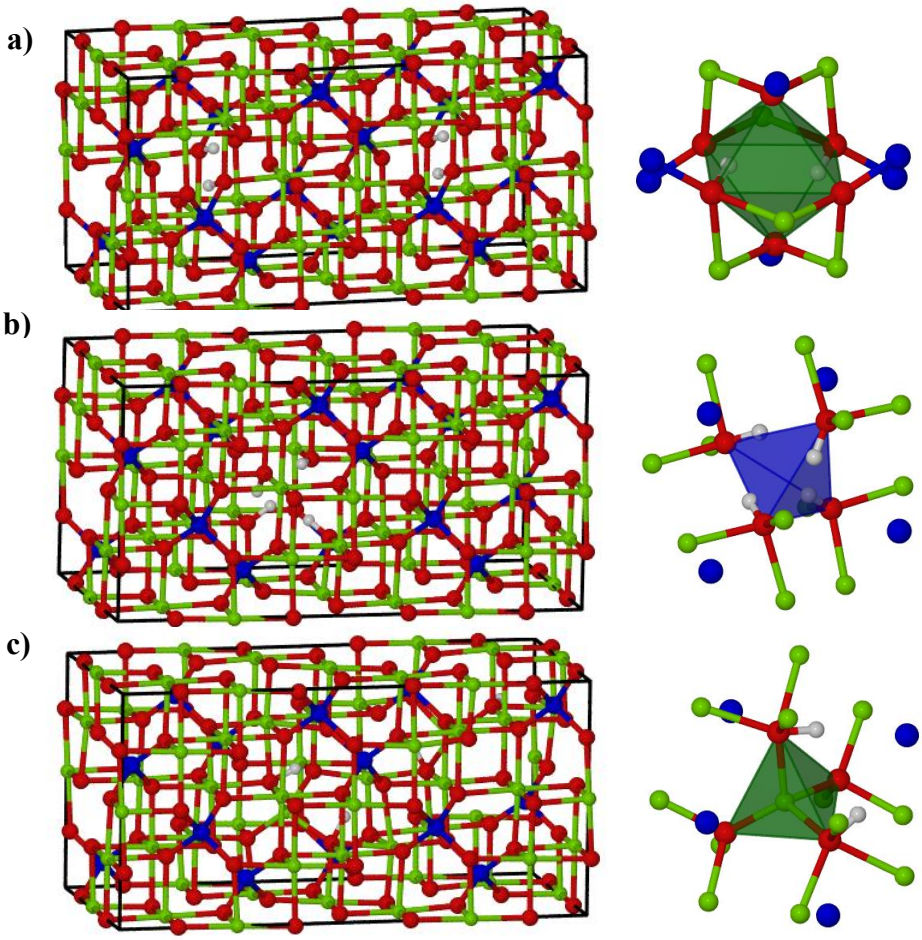

*Figure S5: Isolated defects of the type a) V_{Mg}''+ 2H** (Mg1), b) V_{Si}''''+ 4H**** (Si1) and c) Mg_{Si}''+ 2H** (Mg_{Si}1). The geometry-optimized structure is shown left, while the local coordination of the defect site is shown on the right side.*

Multiple proton configurations (Figure S6) with various hydrogen bond length between ~1.65 and 2.04 Å, all located along the edge between the 16d and 16c octahedra, were found to be stable with a maximum energy difference of about 3.6 kJ/mol to the most stable structure with two hydrogen bonds of 1.67 Å and 1.68 Å.

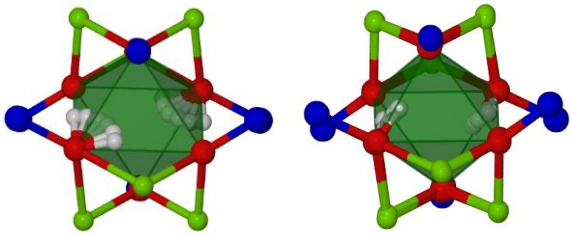

*Figure S6: Left: multiple starting hydrogen positions of the hyxroxyl group for the defect type V_{Mg}''+ 2H**. Right: geometry-optimized positions of the hydroxyl group forming hydrogen bonds along the edge between the 16d and the 16c octahedra.*

Isolated defects of the type V_{Si}''''+ 4H**** (Si1, Figures 3b and S5) were created by removing one Si atom of the 8a tetrahedral site and placing four protons in the vacancy. The resulting hydroxyl groups, which are non-silicate, thus solely coordinated to Mg atoms, form hydrogen bonds close to the tetrahedral edge with the oxygens acting as donor and acceptor. The length of the hydrogen bond is between 2.08 Å and 2.46 Å.
36 V_{Si}''''+ 4H**** defect structures with different hydrogen bond strenghts were simulated with energy differences up to max. ~1.8 kJ/mol (Figure S7). Hereby the hydrogen bond is always located along the tetrahedral edge with varying bond length between 2.05 and 2.43 Å.

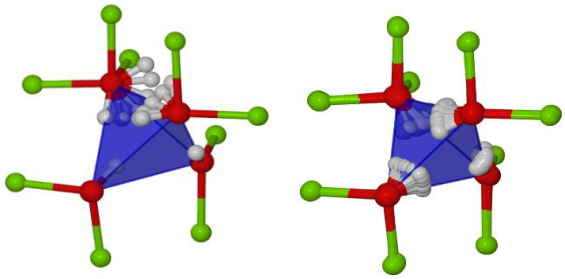

*Figure S7: Left: multiple starting hydrogen positions of the hyxroxyl group for the defect type V_{Si}''''+ 4H**** Right: geometry-optimized positions of the hydroxyl group forming hydrogen bonds along the tetrahedral edges.*

Another kind of Si defect was introduced by the Mg_{Si}''+ 2H** defect type (Mg_{Si}1, Figures 3c and S5). Here, one Si located on the 8a tetrahedral site was replaced by a Mg atom and two protons. In contrast to the simple Si defect (V_{Si}''''+ 4H****) the hydroxyl groups of the Mg_{Si}''+ 2H** defect type are forming hydrogen bonds (1.73 Å - 1.77 Å) along the edges shared by the 16d and 16c octahedra.

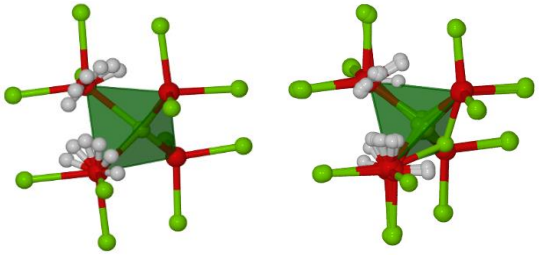

*Figure S8: Left: multiple starting hydrogen positions of the hyxroxyl groups for the defect type Mg_{Si}''+ 2H**. Right: geometry-optimized positions of the hydroxyl group forming hydrogen bonds along between the 16d and the 16c octahedra.*

In the case of the Mg_{Si}''+ 2H** defect type multiple hydrogen bond patterns with energy differences up to ~30 kJ/mol were simulated (Figure S8). Hereby three different types of hydrogen bonding could be clearly distinguished. In the first and energetically favoured case

the hydrogen bond is along the edges shared by the 16d and 16c octahedra and has a length of 1.71-1.78 Å. In the second case the hydrogen bond itself is also along these edges, but is less linear and almost bifurcated between two oxygens forming hydrogen bond lengths of about 1.83-2.03 Å. Here, the energy difference is between 3 kJ/mol and 13 kJ/mol depending not only on the orientation of the bifurcated hydrogen bond but also of the second hydroxyl group. In the third case the hydrogen bond of the hydroxyl group is along the tetrahedral edge. As a result the Mg atom is moving out of the center of the tetrahedron towards the vacant 16c octahedron. The hydrogen bond length along the tetrahedral edge is about 2.14 to 2.20 Å and the energy difference to the most stable structure simulated is about 9 kJ/mol and thus under the synthesis conditions easily accessible.

Three different coupled Mg defects of the type V_{2Mg}````+ 4H**** were created by the removal of two neighboring Mg atoms and adding four protons around the resulting vacancies (Figures 3d and S9). Hereby always two protons were placed close to the oxygen atoms of the sharing edge between the vacancies since a higher partial charge of those oxygen atoms is expected. By variation of the other two protons in the vacant 16d and 16c octahedra around the vacancies three different models were evaluated. In all three cases the hydroxyl groups form hydrogen bonds along the O-O edge between the 16d and 16c octahedra, as in the case of isolated vacancies (V_{Mg}´´+ 2H**). Hereby the hydrogen bond lengths is varying between 1.52 and 2.05 Å. One extremly short hydrogen bond of 1.38 Å does not seem to be realistic and was no further taken into account. The slightly shorter hydrogen bonds in comparison to the isolated Mg defect can be explained by greater distortions in the structure being possible due to the coupled defects.

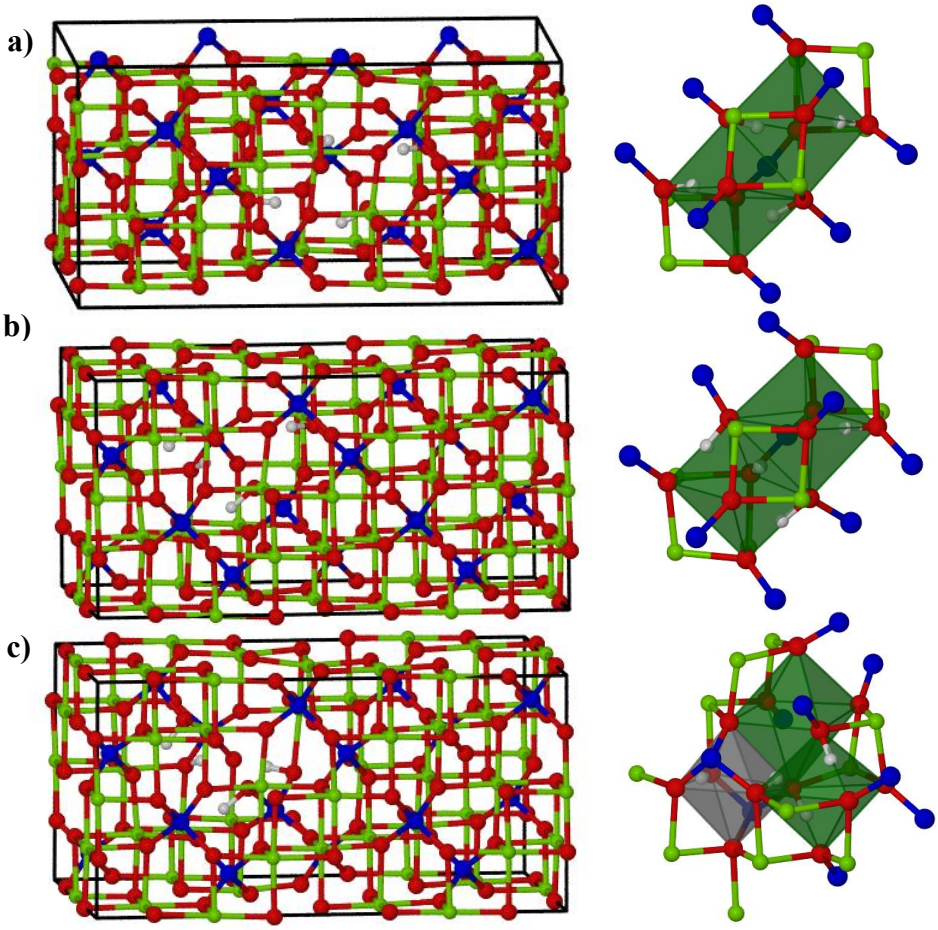

*Figure S9: Coupled Mg defects of the type V_{2Mg}````+ 4H**** with three different proton configurations (a) Mg2_1; b) Mg2_2; c) Mg2_3). The geometry-optimized structure is shown left, while the local coordination of the defect site is shown on the right side. The vacant 16d octahedra are shown in green, while the vacant 16c octahedron is shown in grey.*

Furthermore, five coupled and mixed defect structures with Si and Mg vacancies were considered. This way hydroxyl groups with significantly different cation environment and thus chemical shift in one single defect can be realized and investigated. Here, models with six-coordinated Si atoms (Mg_{Si}``+$Si_{Mg}$** +$V_{Mg}$``+ 2H**, Mg_{Si}-Si_{Mg}-Mg_1-2, Figures 3f and S11), according to models of previous work of Blanchard et al.[6], and without ^{VI}Si atoms ($Mg_{Si}V_{Mg}$````+ 4H****; Mg_{Si}-Mg_1-3, Figures 3e and S10) can be differentiated.

The latter can be described by local cation disorder with a four-coordinated Mg cation on the 8a site directly connected to a vacant 16d site wich is normally occupied by magnesium. This nominally corresponds to a Si defect. The oxygen atom connecting the defects is carrying the highest partial charge in these models and is therefore always forming a hydroxyl group. The configuration of the other three protons needed for charge balance, was varied (Figure S10) resulting in three different models.

All hydroxyl groups of these models, both of the V_{Mg}´´+ 2H** type, as well as the Mg_{Si}``+ 2H** type, are forming hydrogen bonds along the edges between the 16d and 16c octhedra. The hydrogen bond length is varying between 1.71 and 1.81 Å for the hydroxyl groups located in the Mg vacancy (2x Mg and 1x Si cation environment), 1.72 and 1.83 Å for the hydroxyl groups of the $Mg_{Si}$``+ 2H** type (4x Mg cation environment) and between 1.81 and 2.03 Å for the hydroxyl group located on the connecting oxygen atom (3x Mg cation environment).

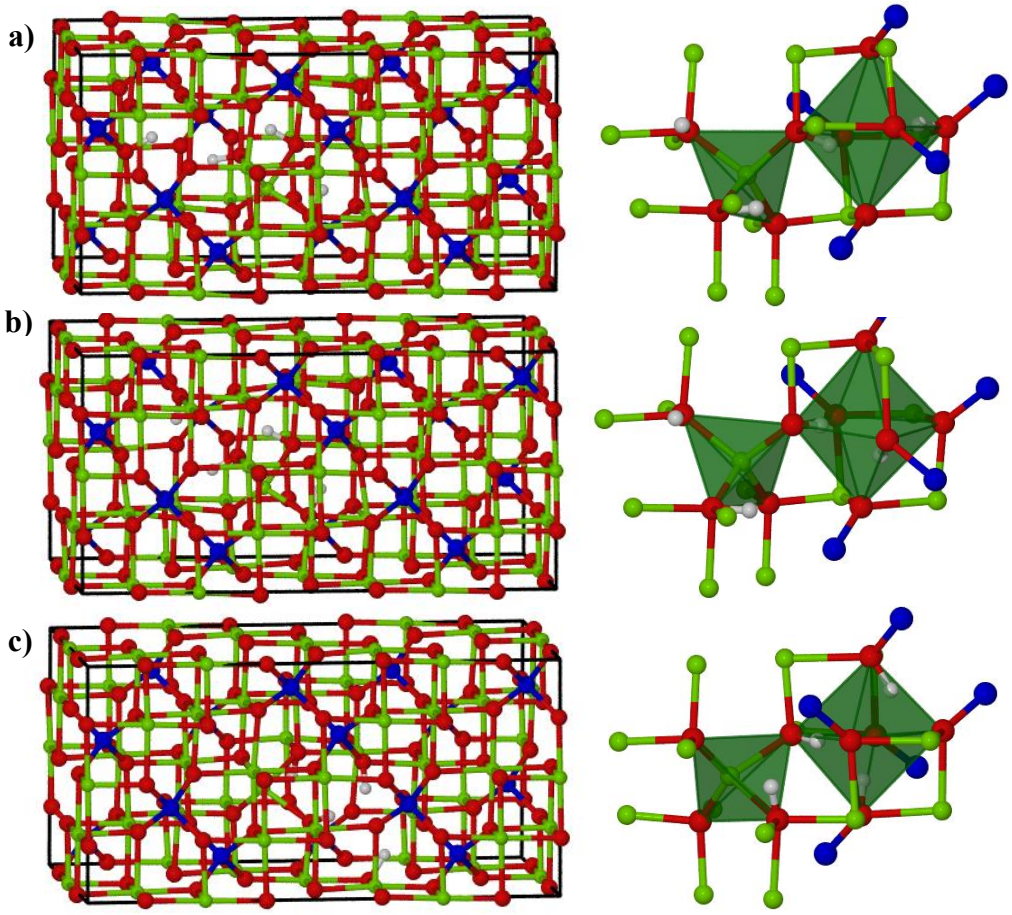

*Figure S10: Coupled mixed defects of the type $Mg_{Si}V_{Mg}$````+ 4H**** with three different proton configurations (a) Mg_{Si}-Mg_1; b) Mg_{Si}-Mg_2; c) Mg_{Si}-Mg_3). The geometry-optimized structure is shown left, while the local coordination of the defect site is shown on the right side.*

Models with a local cation disorder with ^{VI}Si species (Mg_{Si}``+$Si_{Mg}$** +$V_{Mg}$``+ 2H**) are shown in Figures 3f and S11. Here cation disorder between Mg and Si (16d and 8a site) connected to a Mg vacancy, thus a vacant 16d octahedron, was modelled. Again the cornersharing oxygen connecting the Mg_{Si}`` site with the vacant 16d site, is protonated because of its high partial charge. The other proton is located in the vacant 16d site. Both hydroxyl groups of each model form hydrogen bonds along the edge shared by the 16d and 16c octahedra with bond lengths between 1.63 and 1.93 Å, whereby the local cation environment doesn't seem to influence the bond length significantly.

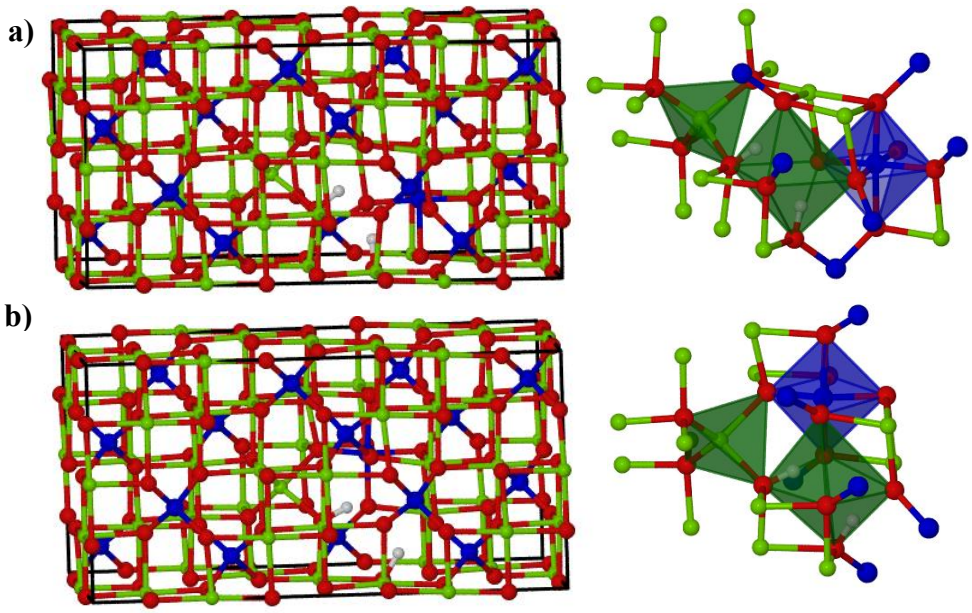

*Figure S11: Coupled mixed defects of the type Mg_{Si}``+$Si_{Mg}$** +$V_{Mg}$``+ 2H** in two different configurations (a) Mg_{Si}-Si_{Mg}-Mg_1; b) Mg_{Si}-Si_{Mg}-Mg_2). The geometry-optimized structure is shown left, while the local coordination of the defect site is shown on the right side.*

The calculated ^{29}Si chemical shifts grouped by the nearest hydrogen environment and the calculated ^{1}H chemical shift, hydrogen bond length and cation environment of the hydroxyl groups of all the different fully geometry-optimized models are summarized in Tables S3 and S4, respectively.

The calculated ^{1}H chemical shifts, the respective OH···O bond length and the energy difference of multiple proton configurations of the isolated models V_{Mg}´´+ 2H**, Mg_{Si}´´+ 2H** and V_{Si}´´´´+ 2H****, shown in Figures S6-8, are listed in Tables S5-7, respectively.

Table S3: Calculated ^{29}Si chemical shift grouped by the closest hydrogen environment for the fully geometry-optimized hydrous defect models (Figure 3a-f).

model	*Defect type*	*δ (^{IV}Si-OH) / ppm*	*δ (^{IV}Si···OH) / ppm*	*δ (^{IV}Si-O) / ppm*	*δ (^{VI}Si-O) / ppm*
Mg1	V_{Mg}''+ 2H**	-78.89 -78.89 -78.89 -78.89	-80.38 -80.38 -80.39 -80.37 -80.38 -80.39 -80.38 -80.38	-81.53 -81.53 -81.52 -81.52	-
Si1	V_{Si}''''+ 4H****	-	-	-81.11 -81.77 -81.87 -81.28 -81.99 -82.06 -81.86 -81.94 -81.51 -80.79 -81.30 -81.98 -81.91 -82.08 -82.00	-
Mg_{Si}1	Mg_{Si}''+ 2H**	-	-	-81.14 -81.67 -81.72 -81.21 -81.69 -82.17 -81.85 -81.01 -80.38 -81.21 -82.03 -81.68 -81.89 -81.85	-
Mg2_1	V_{2Mg}''''+ 4H****	-78.60 -78.49 -77.53 -76.98	-78.91 -79.22 -78.67 -78.5	-80.99 -81.59 -81.61 -81.87 -81.07 -81.66 -81.64 -81.51	-
Mg2_2	V_{2Mg}''''+ 4H****	-78.32 -78.56 -76.36 -76.54	-78.68 -77.96 -78.15	-81.73 -81.46 -81.77 -81.85 -81.02 -81.59 -81.29 -81.51 -81.53	-

model	*Defect type*	*δ (^{IV}Si-OH) / ppm*	*δ (^{IV}Si···OH) / ppm*	*δ (^{IV}Si-O) / ppm*	*δ (^{VI}Si-O) / ppm*
Mg2_3	V_{2Mg}````+ 4H****	-78.15 -76.08	-78.56 -77.53	-81.42 -81.72 -82.08 -81.67 -81.97 -81.29 -81.75 -81.48 -81.23 -81.36 -81.44	-
Mg_{Si}-Mg_1	$Mg_{Si}V_{Mg}$```` + 4H****	-79.09	-80.48 -80.28 -78.57	-80.71 -81.35 -80.78 -81.30 -81.62 -81.97 -82.03 -81.04 -81.15 -81.84 -80.39	-
Mg_{Si}-Mg_2	$Mg_{Si}V_{Mg}$```` + 4H****	-78.48	-79.78 -80.58	-80.81 -81.75 -81.45 -81.40 -81.78 -82.11 -81.90 -81.02 -81.64 -81.63 -80.18	-
Mg_{Si}-Mg_3	$Mg_{Si}V_{Mg}$```` + 4H****	-79.06 -77.81	-79.00 -78.34 -79.16	-81.55 -81.62 -81.40 -80.27 -81.97 -81.17 -80.94 -81.20 -80.98 -81.79 -81.94	-
Mg_{Si}-Si_{Mg}-Mg_1	Mg_{Si}``+$Si_{Mg}$** +$V_{Mg}$``+ 2H**	-81.47	-80.87 -85.61	-81.30 -81.59 -80.83 -81.62 -82.68 -82.03 -81.94 -82.29 -83.84 -83.06 -85.09 -85.61 -82.55 -81.47	-173.57

model	*Defect type*	*δ (^{IV}Si-OH) / ppm*	*δ (^{IV}Si···OH) / ppm*	*δ (^{IV}Si-O) / ppm*	*δ (^{VI}Si-O) / ppm*
Mg_{Si}-Si_{Mg}-Mg_2	Mg_{Si}``+$Si_{Mg}$** +$V_{Mg}$``+ 2H**	-78.91	-78.79 -84.41	-81.66 -80.93 -81.47 -80.49 -81.45 -82.19 -81.73 -81.93 -82.09 -84.41 -83.71 -85.17 -78.91 -82.62	-166.83

Table S4: Calculated ^{1}H chemical shift, hydrogen bond length and cation environment of the hydroxyl groups of the different fully geometry-optimized hydrous defect models in the structure of ringwoodite.

model	*Defect type*	*N (H)*	*Cat.env.* δH_1 *(OH…O length)*	*Cat.env.* δH_2 *(OH…O length)*	*Cat.env.* δH_3 *(OH…O length)*	*Cat.env.* δH_4 *(OH…O length)*
Mg1	V_{Mg}''+ 2H**	4	2x Mg; 1x Si 7.32 ppm (2.04 Å)	2x Mg; 1x Si 7.32 ppm (2.04 Å)	2x Mg; 1x Si 7.32 ppm (2.04 Å)	2x Mg; 1x Si 7.32 ppm (2.04 Å)
Si1	V_{Si}''''+ 4H****	4	3x Mg -0.31 ppm (2.46 Å)	3x Mg 1.76 ppm (2.14 Å)	3x Mg 1.46 ppm (2.15 Å)	3x Mg 1.77 ppm (2.10 Å)
Mg_{Si}1	Mg_{Si}''+ 2H**	4	4x Mg 5.48 ppm (1.73 Å)	4x Mg 5.19 ppm (1.75 Å)	4x Mg 4.98 ppm (1.76 Å)	4x Mg 4.65 ppm (1.77 Å)
Mg2_1	V_{2Mg}''''+ 4H****	4	1x Mg; 1x Si 8.13 ppm (1.75 Å)	1x Mg; 1x Si 8.02 ppm (1.80 Å)	2x Mg; 1x Si 11.77 ppm(1.60 Å)	2x Mg; 1x Si 10.51 ppm(1.67 Å)
Mg2_2	V_{2Mg}''''+ 4H****	4	2x Mg; 1x Si 11.20 ppm (1.63 Å)	1x Mg; 1x Si 11.09 ppm (1.54 Å)	1x Mg; 1x Si 11.92 ppm (1.52 Å)	2x Mg; 1x Si 6.14 (2.05 Å)
Mg2_3	V_{2Mg}''''+ 4H****	4	1x Mg; 1x Si 10.86 ppm (1.55 Å)	1x Mg; 1x Si 15.30 ppm (1.38 Å)	2x Mg; 1x Si 10.95 ppm (1.59 Å)	2x Mg; 1x Si 6.28 ppm (1.98 Å)
Mg_{Si}-Mg_1	$Mg_{Si}V_{Mg}''''$+ 4H****	4	3x Mg 3.4 ppm (2.03 Å)	4x Mg 5.43 ppm (1.76 Å)	4x Mg 5.75 ppm (1.74 Å)	2x Mg; 1x Si 9.40 ppm (1.73 Å)
Mg_{Si}-Mg_2	$Mg_{Si}V_{Mg}''''$+ 4H****	4	3x Mg 4.71 ppm (1.88 Å)	2x Mg; 1x Si 8.14 ppm (1.81 Å)	4x Mg 5.42 ppm (1.74 Å)	4x Mg 6.25 ppm (1.72 Å)
Mg_{Si}-Mg_3	$Mg_{Si}V_{Mg}''''$+ 4H****	4	2x Mg; 1x Si 9.37 ppm (1.71 Å)	2x Mg; 1x Si 9.52 ppm (1.72 Å)	4x Mg 4.26 ppm (1.83 Å)	3x Mg 4.57 ppm (1.81 Å)
Mg_{Si}-Si_{Mg}-Mg_1	Mg_{Si}''+Si_{Mg}** +V_{Mg}''+ 2H**	2	3x Mg 4.57 ppm (1.80 Å)	2x Mg; 1x Si 7.51 ppm (1.86 Å)	-	-
Mg_{Si}-Si_{Mg}-Mg_2	Mg_{Si}''+Si_{Mg}** +V_{Mg}''+ 2H**	2	3x Mg 3.00 ppm (1.93 Å)	2x Mg; 1x Si 10.69 ppm (1.63 Å)	-	-

*Table S5: Calculated hydrogen bond length and ^1H chemical shift of the hydroxyl groups, as well as relative energies of the multiple proton configurations of the model Mg1 (V_{Mg}'' + 2H**). The cation environment of all the hydroxyl groups is 2x Mg and 1x Si.*

Proton conf. No.	*r(OH…O) H1 / Å*	*δ (H1) / ppm*	*r(OH…O) H2 / Å*	*δ (H2) / ppm*	*ΔE / kJ/mol*
1	1.75	9.04	1.69	9.81	2.32
2	1.74	9.06	1.72	9.36	2.25
3	1.73	9.22	1.77	8.74	2.40
4	1.72	9.33	1.93	7.49	3.59
5	1.67	10.14	1.68	9.99	0.02
6	1.70	9.61	1.70	9.62	0.25
7	1.72	9.31	1.73	9.22	2.17
8	1.73	9.27	1.70	9.68	2.21
9	1.74	9.10	1.69	9.85	2.28
10	1.70	9.70	1.75	9.07	2.28
11	1.68	10.03	1.68	10.04	0.03
12	1.68	10.02	1.67	10.11	0.00
13	1.68	9.94	1.69	9.84	0.05
14	1.68	9.97	1.67	10.09	0.00
15	1.69	9.82	1.65	10.43	0.14
16	1.68	10.06	1.68	10.04	0.07
17	1.72	9.38	1.72	9.43	2.17
18	1.93	7.49	1.72	9.33	3.60
19	1.68	9.92	1.68	10.01	0.04
20	1.70	9.69	1.68	9.92	0.12
21	1.68	9.92	1.68	9.92	0.10
22	1.66	10.33	1.68	9.93	0.07
23	1.72	9.44	1.72	9.37	2.16
24	1.77	8.74	1.73	9.23	2.39
25	1.70	9.76	1.67	10.12	0.15
26	1.70	9.76	1.70	9.75	0.17
27	1.68	9.92	1.70	9.69	0.12
29	1.67	10.11	1.68	10.01	0.02
30	1.74	9.37	1.72	9.07	2.25
31	1.67	10.10	1.67	10.10	0.12
32	1.67	10.12	1.70	9.75	0.15
33	1.68	10.01	1.68	9.92	0.04
34	1.69	9.84	1.68	9.93	0.06
35	1.73	9.22	1.72	9.34	2.16
36	1.69	9.81	1.75	9.04	2.32

*Table S6: Calculated hydrogen bond length and ^{1}H chemical shift of the hydroxyl groups, as well as relative energies of the multiple proton configurations of the model $Mg_{Si}1$ (Mg_{Si}''+ 2H**). The cation environment of all the hydroxyl groups is 4x Mg.*

Proton conf. No.	*r(OH…O) H1 / Å*	*δ (H1) / ppm*	*r(OH…O) H2 / Å*	*δ (H2) / ppm*	*ΔE / kJ/mol*
1	1.75	4.62	1.75	5.43	11.20
2	1.74	4.84	1.77	5.17	11.56
3	1.73	5.04	1.72	5.86	10.61
4	1.73	4.89	1.72	5.85	10.74
5	1.67	6.24	1.68	6.11	29.59
6	1.68	6.14	1.67	6.19	29.53
7	1.75	4.84	1.78	4.39	3.42
8	1.76	4.82	1.87	3.61	3.93
9	1.76	4.83	1.76	4.79	0.07
10	1.76	4.77	1.76	4.80	0.06
11	1.72	5.84	1.72	5.12	10.55
12	1.71	6.08	1.71	5.19	10.56
13	1.75	4.86	1.77	4.48	3.39
14	1.75	4.85	1.92	3.39	4.13
15	1.76	4.83	1.76	4.89	0.10
16	1.76	4.82	1.76	4.76	0.12
17	1.73	5.79	1.72	5.02	10.58
18	1.71	6.07	1.71	5.20	10.69
19	1.74	5.02	1.78	4.36	3.43
20	1.76	4.82	1.76	4.88	0.00
21	1.76	4.90	1.76	4.80	0.14
22	1.76	4.85	1.76	4.83	0.00
23	1.74	4.40	1.9	4.85	12.74
24	1.96	4.26	1.73	5.00	13.03
25	1.77	4.74	1.76	4.89	0.00
26	1.83	3.90	1.75	4.97	3.57
27	1.78	4.29	1.75	4.99	3.44
28	1.78	4.32	1.76	4.82	3.30
29	1.75	5.44	1.75	4.68	11.14
30	1.74	5.50	1.74	4.77	11.35
31	1.75	4.80	1.74	5.08	2.61
32	1.75	4.81	1.75	5.00	2.58
33	1.77	4.46	1.75	4.87	3.34
34	1.78	4.42	1.75	4.96	3.40
35	2.03	3.39	2.2	2.25	9.00
36	1.74	5.51	1.75	4.74	11.23

*Table S7: Calculated hydrogen bond length and ^1H chemical shift of the hydroxyl groups, as well as relative energies of the multiple proton configurations of the model Si1 ($V_{Si}^{\prime\prime\prime}$+ 4H****). The cation environment of all the hydroxyl groups is 3x Mg.*

Proton conf. No.	*r(OH…O) H1 / Å*	*δ(H1) / ppm*	*r(OH…O) H2 / Å*	*δ(H2) / ppm*	*r(OH…O) H3 / Å*	*δ(H3) / ppm*	*r(OH…O) H4 / Å*	*δ(H4) / ppm*	*ΔE / kJ/mol*
1	2.16	0.86	2.14	0.73	2.09	1.99	2.33	0.94	0.41
2	2.22	0.21	2.11	1.29	2.08	2.02	2.22	1.28	0.07
3	2.37	-0.22	2.15	1.38	2.08	1.81	2.13	1.76	0.35
4	2.34	-0.19	2.18	1.35	2.08	1.62	2.10	1.95	0.31
5	2.24	0.10	2.10	1.22	2.08	1.33	2.23	2.05	0.12
6	2.16	0.61	2.30	1.02	2.16	0.94	2.08	1.97	0.28
7	2.22	0.63	2.14	0.81	2.09	1.91	2.34	0.91	0.76
8	2.27	-0.01	2.09	1.46	2.08	2.03	2.19	1.38	0.15
9	2.43	-0.29	2.12	1.63	2.09	1.74	2.10	1.90	0.40
10	2.33	-0.19	2.15	1.61	2.10	1.51	2.07	2.03	0.27
11	2.24	0.16	2.21	1.35	2.16	1.09	2.08	1.87	0.30
12	2.21	0.42	2.26	1.13	2.23	0.70	2.09	1.80	0.76
13	2.30	0.30	2.14	0.94	2.13	1.64	2.39	0.73	1.12
14	2.43	-0.21	2.08	1.64	2.10	1.88	2.16	1.43	0.26
15	2.43	-0.34	2.12	1.70	2.12	1.57	2.10	1.66	0.29
16	2.34	-0.14	2.14	1.75	2.15	1.37	2.07	1.85	0.32
17	2.27	0.15	2.18	1.45	2.20	1.05	2.08	1.76	0.67
18	2.26	0.30	2.21	1.26	2.30	0.59	2.11	1.51	1.14
19	2.24	0.49	2.14	1.34	2.23	1.05	2.38	0.50	1.79
20	2.28	-0.02	2.07	1.95	2.18	1.50	2.12	1.36	0.22
21	2.33	-0.12	2.10	1.91	2.20	1.24	2.08	1.55	0.34
22	2.37	0.00	2.13	1.77	2.23	1.02	2.08	1.62	0.49
23	2.33	0.12	2.17	1.55	2.29	0.77	2.10	1.53	0.90
24	2.33	0.30	2.18	1.36	2.39	0.63	2.15	1.09	1.58
25	2.13	1.18	2.14	1.62	2.37	0.73	2.35	0.18	1.57
26	2.17	0.59	2.07	2.15	2.33	1.00	2.11	1.13	0.08
27	2.27	0.24	2.10	1.90	2.34	0.83	2.10	1.18	0.55
28	2.31	0.26	2.13	1.68	2.39	0.73	2.12	1.16	0.88
29	2.38	0.35	2.16	1.45	2.35	0.74	2.17	0.92	1.48
30	2.39	0.53	2.15	1.21	2.23	1.15	2.28	0.39	1.88
31	2.12	1.20	2.14	1.69	2.35	0.71	2.32	0.21	1.33
32	2.15	0.67	2.08	2.14	2.34	0.97	2.11	1.10	0.00
33	2.25	0.33	2.11	1.91	2.36	0.84	2.10	1.21	0.44
34	2.34	0.29	2.14	1.60	2.39	0.75	2.14	0.94	1.16
35	2.39	0.42	2.16	1.38	2.32	0.78	2.20	0.74	1.70
36	2.39	0.61	2.15	1.15	2.20	1.25	2.33	0.33	1.79

S5. References

(1) Sasaki, S.; Prewitt, C. T.; Sato, Y.; Ito, E. *J. Geophys. Res.* **1982**, *87*, 7829.
(2) Ross, N. L.; Shu, J.-F.; Hazen, R. M.; Gasparik, T. *Am. Mineral.* **1990**, *75* (7–8), 739.
(3) Kahler, H. *Phys. Rev.* **1921**, *18*, 210.
(4) Kristiansen, P. E.; Carravetta, M.; van Beek, J. D.; Lai, W. C.; Levitt, M. H. *J. Chem. Phys.* **2006**, *124* (23), 234510.
(5) Kristiansen, P. E.; Mitchell, D. J.; Evans, J. N. S. *J. Magn. Reson.* **2002**, *157* (2), 253.
(6) Blanchard, M.; Balan, E.; Wright, K. *Am. Mineral.* **2009**, *94*, 83.